Journal of Catalysis 258 (2008) 306–314

Contents lists available at ScienceDirect

Journal of Catalysis

www.elsevier.com/locate/jcat

Pt_3Co and PtCu intermetallic compounds: Promising catalysts for preferential oxidation of CO in excess hydrogen

Takayuki Komatsu *, Asako Tamura

Department of Chemistry, Tokyo Institute of Technology, 2-12-1-E1-10 Ookayama, Meguro-ku, Tokyo 152-8550, Japan

ARTICLE INFO

Article history:
Received 14 April 2008
Revised 2 June 2008
Accepted 2 June 2008

Keywords:
Preferential oxidation
Carbon monoxide
Hydrogen
Intermetallic compound
Platinum
Cobalt
Copper

ABSTRACT

Pt-based intermetallic compounds (IMCs) supported on silica were studied as a catalyst for the preferential oxidation (PROX) of CO in excess hydrogen to obtain the active catalyst at low temperatures. Pt_3Co/SiO_2 and $PtCu/SiO_2$ were more active than Pt/SiO_2 and Pt/Al_2O_3 in the temperature range of 373–453 K. Both IMC catalysts were stable during the reaction at 473 K without the irreversible segregation at the surface. Infrared (IR), X-ray photoelectron spectroscopy (XPS), and adsorption measurements revealed a significant electron transfer from Pt atoms to Co or Cu atoms. The electron-deficient Pt atoms adsorbed CO weakly compared with Pt metal, accelerating the adsorption of oxygen on the IMC surface. Kinetic studies indicated that Co and Cu atoms in IMCs also adsorb oxygen. This improved oxygen adsorption likely resulted in the high PROX activity at low temperatures. The effects of hydrogen and water on the rate of CO_2 formation also were studied.

1. Introduction

Preferential oxidation of CO in an excess amount of hydrogen (PROX) is an important process for obtaining CO-free hydrogen for proton exchange membrane fuel cells (PEMFCs). Hydrogen produced through the steam reforming of hydrocarbons, such as naphtha and natural gas, always contains CO as a byproduct at a level of 10–20%. The water–gas shift reaction is applied to reduce the CO concentration in hydrogen. But a significant amount of CO (ca. 1%) remains in hydrogen to deactivate the platinum electrodes of PEMFCs. The PROX of CO further reduces the proportion of CO to $\leqslant$10 ppm, providing sufficient life for PEMFCs.

Supported platinum catalysts have been widely studied for the PROX reaction. Oh and Sinkevitch [1] reported that Pt was the most active among various metals supported on alumina at higher temperatures (around 440 K). However, from an economical standpoint, drawbacks of Pt catalysts include their low activity at temperatures around 370 K (the operating temperature of PEMFCs) and their low selectivity to CO_2 due to the higher oxygen concentration to increase the activity. Consequently, bimetallic catalysts containing Pt and a second element have been studied in efforts to improve the activity of Pt catalysts. The activity of $Pt–Ru/SiO_2$ was found to be between the activities of Pt/SiO_2 and Ru/SiO_2 [2], although the addition of Pt improved the dispersion of Ru. Pt–Au supported on zeolite-A with an Pt/Au atomic ratio of 2 has been found to be the most active Pt–Au/A catalyst [3]. In this catalyst, Pt and Au appeared to be in separated phases. In the case of $Pt–Pd/CeO_2$ [4], the most active catalyst had the composition of Pt/Pd = 1/7. $Pt–Ni/Al_2O_3$ prepared by co-impregnation proved to be a better catalyst than that prepared by successive impregnation [5]. EDX revealed the presence of Pt–Ni bimetallic particles with a Pt/Ni ratio of 0.5–2 and monometallic Ni particles. Co-impregnation tended to create the bimetallic particles, which may be the active species at lower temperatures. The foregoing combinations of Pt and other metals have solid solution phases with widely ranging compositions [6].

Intermetallic compounds (IMCs) are the stoichiometric compounds between two or more metal elements. Compared with typical alloys, which are solid solutions with the same crystal structures as their component metals, various IMCs have different specific crystal structures than those of their component metals. Therefore, some IMCs are known to have unique bulk properties, such as superconductivity, hydrogen storage ability, and shape memory effects. The catalytic properties of IMCs have been little studied to date, except in the so-called “hydrogen storage alloys,” such as $LaNi_5$ [7]. We have previously studied the catalytic properties of IMCs compared with those of pure metals [8–16]. When Pt-based IMCs were used for $H_2–D_2$ equilibration, Pt_3Ge, Pt_2Ge, and PtGe gave much lower activity than Pt [9], and Pt_3Ti and $PtTi_3$ gave much higher activity than Pt [13]. Pt_3Ge was highly selective for the partial hydrogenation of 1,3-butadiene into butenes [9]. Pt_3Ti was more active than Pt for the hydrogenation of ethylene [13].

* Corresponding author. Fax: +81 3 5734 2758.
E-mail address: komatsu@chem.titech.ac.jp (T. Komatsu).

0021-9517/$ – see front matter
doi:10.1016/j.jcat.2008.06.030

Pt_3Sn/H-SAPO-11 was more selective than Pt/H-SAPO-11 for the dehydroisomerization of butane into isobutene [16]. The formation of Pt_3Sn retarded the hydrogenolysis to methane without decreasing the dehydrogenation activity, resulting in increased selectivity to isobutene. The similar retardation of hydrogenolysis also was observed for the aromatization of butane on Pt_3Ge/H-ZSM-5 compared with Pt/H-ZSM-5 [11].

In the foregoing cases, the formation of IMCs drastically changed the adsorption behavior from pure Pt metal through changes in the atomic distance between the Pt atoms and the electronic state of Pt. Therefore, on the surface of IMCs, the adsorption of CO and O_2, as well as hydrogen, can be altered by forming IMCs with other elements. This will change the catalytic properties of Pt for the PROX reaction. To date, however, the catalytic properties of single-phase IMCs for PROX have not been reported.

In recent years, Pt-based bimetallic catalysts, in which Pt and the other element can have IMC phases without forming the wide-range solid solution phases, have been studied for the PROX reaction. Schubert et al. [17] have reported the higher activity and selectivity of Pt–Sn/carbon compared with Pt/Al_2O_3 at 353 K. XPS and IR measurements revealed that most of the tin was present in the oxidized state, SnO_x, although some was reduced to form a Pt–Sn solid solution. It was suggested that this SnO_x species adsorbed oxygen instead of Pt. In the case of Pt–Sn/Nb_2O_5 [18], however, the addition of tin did not enhance the PROX activity. Among the Pt–Co catalysts, Pt–Co/TiO_2 was reportedly more active than Pt/TiO_2 at low temperatures [19]. XPS and TPR results demonstrated Co species in various oxidation states. Pt–Co/Al_2O_3 with Pt/Co = 1 also was more active than Pt/Al_2O_3 [20]; however, the active species were not identified by XRD measurements. The addition of sodium on Pt–Co/Al_2O_3 promoted the formation of a Pt–Co bimetallic phase, inhibiting cobalt spinel formation on the surface [21]. On a YSZ support [22], the catalyst with Pt/Co = 1/5 was the most active. TEM of this catalyst revealed isolated Pt–Co bimetallic particles, as well as cobalt particles. Watanabe et al. [23] found that Pt–Fe/mordenite was more active than Pt/mordenite and Pt/Al_2O_3. They also found that the active catalyst contained metal particles inside the pores of mordenite, where XRD did not reveal the presence of Pt–Fe IMCs [24]. The addition of a large amount of iron onto Pt/TiO_2, where the iron loading corresponded to the comparable amount of TiO_2, also increased the activity at temperatures below 373 K [25]; however, iron was in an oxidized state without the formation of IMCs. In the foregoing studies, the catalytic properties of Pt-based IMCs for PROX were not clarified, although the surface formation of IMCs may contribute to the generation of new active sites.

In the present study, we applied some single-phase Pt-based IMCs to the catalyst for the PROX reaction. Our aim was to clarify the catalytic properties of Pt-based IMCs for the PROX reaction and to obtain IMC catalysts that are active and selective for the formation of CO_2 at lower temperatures.

2. Experimental

2.1. Catalyst preparation

Pt/SiO_2 was prepared by a pore-filling impregnation method. An aqueous solution of tetraammineplatinum(II) acetate (N.E. Chemcat Corp.) was added to silica gel (Cariact G-6, Fuji Silysia) that had been previously dried at 403 K and cooled in air to room temperature. The amount of Pt solution was calculated to fill the pores of silica gel and to achieve a Pt loading of 3 wt%. The mixture was sealed with a piece of plastic film overnight at room temperature, then dried on a hot water bath with stirring and placed into an oven. The temperature was raised in air to 403 K for 6 h and 673 K for 4 h. The Pt/SiO_2 thus prepared was placed into a quartz reactor, into which hydrogen (99.9995%) was fed at a flow rate of 60 ml min^{-1}. After the catalyst was heated at 403 K for 1 h, the temperature was raised to 673 K and kept at this temperature for 2 h to reduce platinum. The catalyst was cooled to room temperature with flowing helium (99.999%) and kept in a drying desiccator.

IMC catalysts, Pt_nM_m/SiO_2 (M = Tl, Cu and Fe), were prepared by successive impregnation onto Pt/SiO_2. In the case of Pt_3Tl_2/SiO_2, a known amount of Pt (3 wt%)/SiO_2 was placed into an evaporating dish, and an aqueous solution of thallium(I) nitrate was added onto the Pt/SiO_2 in an amount corresponding to Pt/Tl = 3/2 (atomic ratio) with the pore-filling procedure. This was sealed with plastic film, left overnight at room temperature, and then reduced similarly to the preparation of Pt/SiO_2 described earlier. In the cases of $PtCu/SiO_2$ and Pt_3Fe/SiO_2, aqueous solutions of copper(II) nitrate and iron(III) nitrate, respectively, were impregnated onto Pt/SiO_2. The reduction temperatures were 873 K for Pt_3Tl_2/SiO_2 and Pt_3Fe/SiO_2 and 1073 K for $PtCu/SiO_2$. The preparation of Pt–Cu/SiO_2 with various Pt/Cu ratios was carried out through a similar impregnation onto Pt (3 wt%)/SiO_2 using a specific amount of copper(II) nitrate solution. Pt_3Co/SiO_2 was prepared by a co-impregnation method. An aqueous solution of tetraammineplatinum(II) acetate and cobalt(II) nitrate was added to silica gel with the pore-filling procedure to achieve the platinum loading of 3 wt% and Pt/Co = 3. The mixture was sealed by the plastic film overnight at room temperature. It was reduced at 673 K by the flowing hydrogen. The preparation of Pt–Co/SiO_2 with various Pt/Co ratios was done by a similar co-impregnation to obtain the Pt loading corresponding to Pt (3 wt%)/SiO_2.

Pt_3Sn/SiO_2 and $PtGe/SiO_2$ were prepared by a chemical vapor deposition (CVD) method with Pt (3 wt%)/SiO_2. Pt/SiO_2 stored in air was placed into a CVD reactor and reduced with flowing hydrogen at 673 K for 30 min. In the case of Pt_3Sn/SiO_2, $Sn(CH_3)_4$ (Soekawa Chemicals) vaporized at 273 K was introduced with a hydrogen carrier (30 ml min^{-1}) at the CVD temperature of 453 K for 1 h to obtain a Pt/Sn ratio of ca. 3. In the case of $PtGe/SiO_2$, $Ge(CH_3)_4$ (Soekawa Chemicals) vaporized at 273 K was used for CVD treatment onto Pt/SiO_2 at the CVD temperature of 553 K for 1 h to obtain a Pt/Ge ratio of ca. 1.

Unsupported IMC catalysts were prepared by melting the mixture of stoichiometric amounts of two component metals in an arc-melting apparatus under 53 kPa of argon. The ingots thus obtained were crushed in air and filtered into particles with diameters <90 μm.

2.2. Characterization

The crystal structure of supported metal particles was examined by powder X-ray diffraction (XRD) using a Rigaku RINT2400 diffractometer with a Cu$K\alpha$ X-ray source. Images were recorded with a JEOL JEM-2010 transmission electron microscope. XPS spectra were recorded with a PerkinElmer PHI 5600 spectrometer. The catalyst was pressed into a pellet and placed into a quartz reactor, where it was reduced under flowing hydrogen. The reduced catalyst was transferred to the spectrometer without being exposed to air. Spectra were obtained with an Al$K\alpha$ X-ray source using C 1s as a reference for binding energy.

IR spectra of adsorbed CO were measured with a JASCO FT/IR-430 spectrometer in transmission mode. A self-supporting wafer (ca. 10 mg cm^{-2}) of catalyst was placed in a quartz cell with CaF_2 windows and attached to a glass circulation system. The catalyst was reduced at 673 K for 30 min with 15 kPa of circulating hydrogen through a cold trap kept at 77 K. Then the catalyst was cooled in vacuo to 298 K, and CO (2 kPa) was introduced for 10 min. After the evacuation at 298 K for 10 min, a spectrum was recorded.

The amount of adsorbed CO was measured with a pulse reaction system. A known amount of catalyst was placed into the

quartz reactor and reduced at 673 K for 1 h with flowing hydrogen. The catalyst was purged by flowing helium at 673 K for 30 min. Pulses of CO (5.0%)/He were introduced with a helium carrier at room temperature, and the outlet gas was analyzed with a thermal conductivity detector to measure the amount of irreversibly adsorbed CO.

2.3. Catalytic reaction

PROX reaction was carried out with a continuous-flow reaction system under atmospheric pressure. A specific amount (0.050 g) of catalyst mixed with 0.1 g of α-alumina was placed into a 17-mm-i.d. quartz tubular reactor. Before the catalytic run, the catalyst was reduced with flowing hydrogen at 673 K for 30 min, then purged by flowing helium at 673 K. The reaction was started at a specific temperature by supplying a reactant gas composed of CO (2.0%), O_2 (1.0–2.0%), H_2 (35%), and He (balance) with a total flow rate of 140 ml min^{-1}. The reaction temperature was raised stepwise, with a product analysis conducted at each temperature. Gaseous products were analyzed with an online gas chromatograph (Shimadzu, GC-14B) with a thermal conductivity detector and a column (2 mm i.d., 3 m long) of active carbon (GL Science). CO_2 selectivity was calculated based on the total amount of oxygen converted into CO_2 and H_2O.

3. Results and discussion

3.1. PROX reaction on Pt-based IMC catalysts

The PROX reaction was carried out with various Pt-based IMCs supported on silica gel. To obtain particles of single-phase IMC, the interaction between metal and support cannot be too strong, because an overly strong interaction will prevent two metal components from forming their compound. Therefore, we selected silica gel (which usually has a very weak interaction with metals) as the support material, even though Pt supported on alumina has been more widely used for oxidation reactions compared with Pt on silica. Fig. 1 shows XRD patterns of Pt–M/SiO_2 (M = Ge, Tl, Cu, Sn, Fe and Co) catalysts prepared with an Pt/M atomic ratio adjusted to the composition of a typical IMC between Pt and M. The parent Pt/SiO_2 (a) showed two diffraction peaks attributed to Pt metal shown in dotted lines. Among Pt–M/SiO_2 catalysts, Pt–Fe (c), Pt–Cu (e) and Pt–Tl (f) on SiO_2 prepared by the successive impregnation gave the single-phase IMCs Pt_3Fe, PtCu, and Pt_3Tl_2, respectively. The co-impregnation gave the single-phase Pt_3Co on SiO_2 (b). On the other hand, these impregnation methods could not obtain single-phase Pt–Sn and Pt–Ge IMCs, whereas the CVD method provided the single-phase Pt_3Sn (d) and PtGe (g). Although the preparation method was not the same, XRD revealed that all of the Pt–M/SiO_2 catalysts had single-phase IMC particles and were free from Pt particles.

These catalysts were tested for the PROX reaction at various temperatures, as shown in Fig. 2 together with the results for Pt/SiO_2. All of the catalysts had the same amount of Pt (1.5 mg). On Pt/SiO_2, the oxidation of CO occurred at temperatures above 420 K. CO conversion increased with reaction temperature, reaching 100% at 493 K. All of the IMC catalysts demonstrated greater CO conversions than Pt/SiO_2 at 453 K and below. Pt_3Co/SiO_2 and PtCu/SiO_2 exhibited conversions of about 60% at 373 K and 100% and 94%, respectively, at 453 K, whereas CO conversion did not increase at temperatures above 453 K on Pt_3Tl_2/SiO_2, Pt_3Fe/SiO_2, and Pt_3Sn/SiO_2. These results indicate that Pt_3Co and PtCu IMCs are better catalysts than Pt for the PROX reaction. In fact, a separate run on Pt (3 wt%)/γ-Al_2O_3 gave CO conversions of only 1% at 373 K and 21% at 413 K.

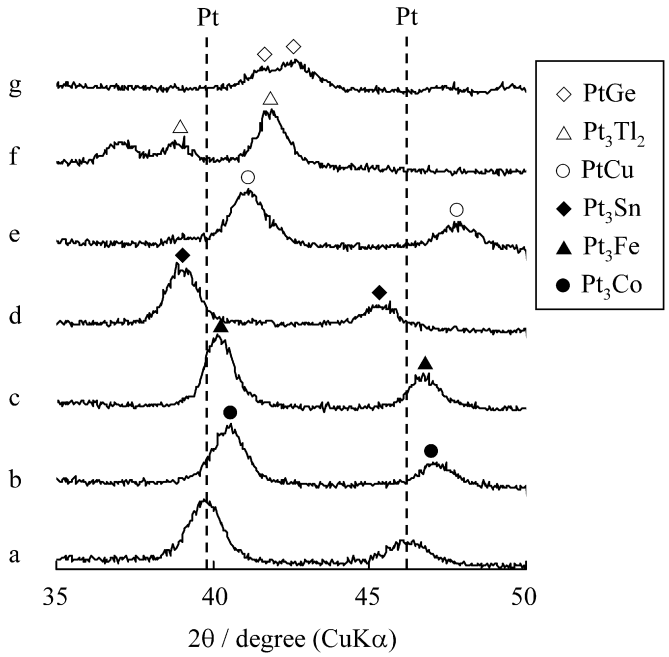

Fig. 1. XRD patterns of Pt (a), Pt–Co (Pt/Co = 3) (b), Pt–Fe (Pt/Fe = 3) (c), Pt–Sn (Pt/Sn = 3) (d), Pt–Cu (Pt/Cu = 1) (e), Pt–Tl (Pt/Tl = 3/2) (f) and Pt–Ge (Pt/Ge = 1) (g) supported on SiO_2.

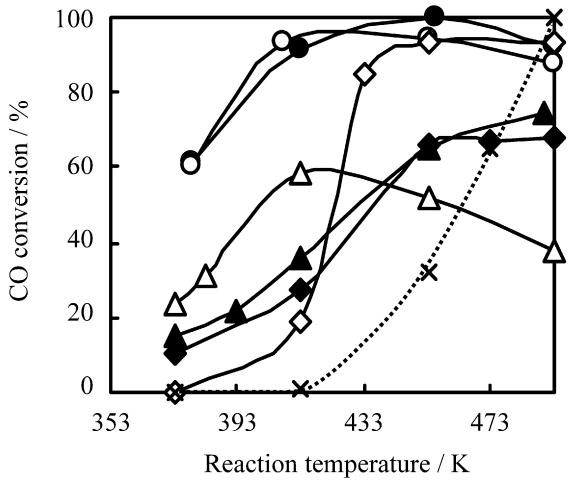

Fig. 2. PROX of CO on Pt (×), Pt_3Co (●), PtCu (○), Pt_3Tl_2 (△), Pt_3Fe (▲), Pt_3Sn (◆) and PtGe (◇) supported on SiO_2. Reactant mixture: CO (2.0%), O_2 (2.0%), H_2 (35%) and He (balance).

3.2. PROX reaction on Pt_3Co/SiO_2 and PtCu/SiO_2

As discussed in the previous section, Pt_3Co and PtCu supported on silica were found to be excellent catalysts for the PROX reaction. Because the combinations of both Pt–Co [26] and Pt–Cu [27] have several IMC phases in their phase diagrams, we evaluated the effect of composition in Pt–Co/SiO_2 and Pt–Cu/SiO_2 on catalytic activity. Fig. 3 shows the CO conversions for Pt–Co/SiO_2 catalysts with Pt/Co atomic ratios of 1/4, 1, 3, 4, and 9. It is clear that all of the Pt–Co/SiO_2 catalysts showed higher CO conversions than Pt/SiO_2. At temperatures below 400 K, Pt–Co/SiO_2 with Pt/Co = 1 gave the highest conversion. But the conversion decreased at higher temperatures, indicating that the selectivity for CO_2 formation must be low at these temperatures. The Co-rich catalyst, Pt–Co/SiO_2 (Pt/Co = 1/4), also exhibited low conversion at high temperatures, although Pt–Co/YSZ (Pt/Co = 1/5) has been re-

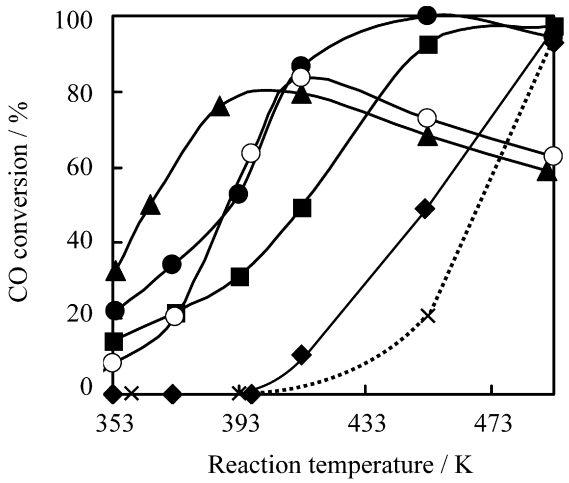

Fig. 3. PROX of CO on Pt–Co/SiO_2 with Pt/Co atomic ratios of 1/4 (○), 1 (▲), 3 (●), 4 (■) and 9 (◆) and on Pt/SiO_2 (×). Reactant mixture: CO (2.0%), O_2 (1.5%), H_2 (35%) and He (balance).

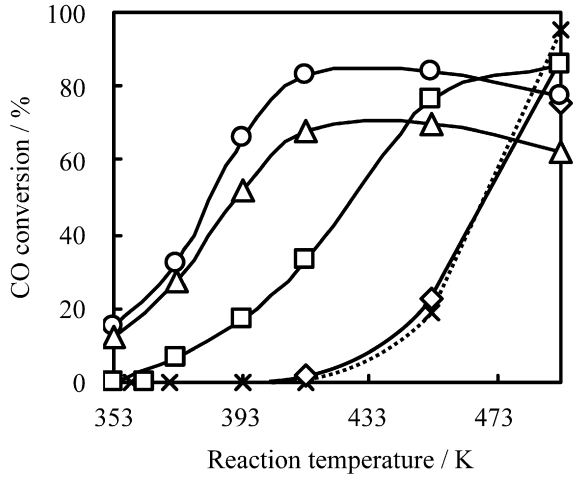

Fig. 5. PROX of CO on Pt–Cu/SiO_2 with Pt/Cu atomic ratios of 0.3 (△), 1 (○), 2 (□) and 5 (◇) and on Pt/SiO_2 (×). Reactant mixture: CO (2.0%), O_2 (1.5%), H_2 (35%) and He (balance).

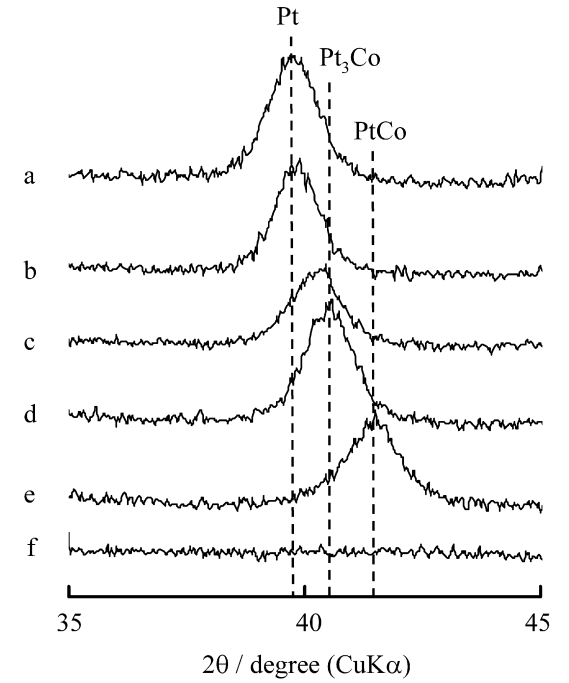

Fig. 4. XRD patterns of Pt/SiO_2 (a) and Pt–Co/SiO_2 with Pt/Co atomic ratios of 9 (b), 4 (c), 3 (d), 1 (e) and 1/4 (f).

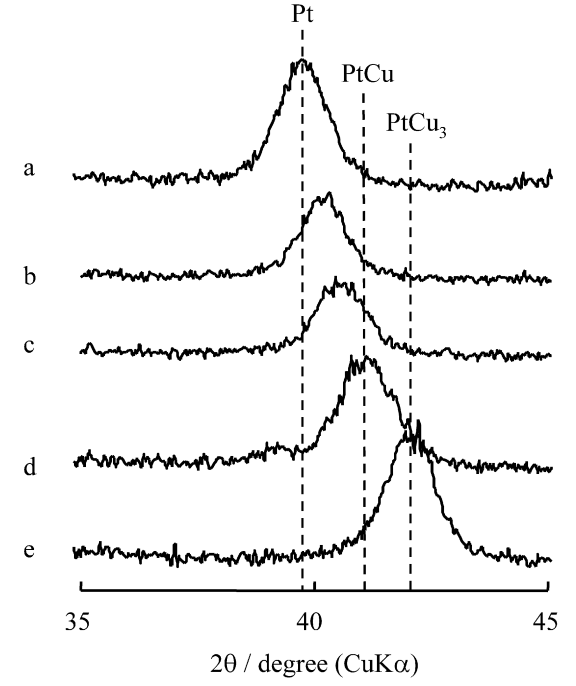

Fig. 6. XRD patterns of Pt/SiO_2 (a) and Pt–Cu/SiO_2 with Pt/Cu atomic ratios of 5 (b), 2 (c), 1 (d) and 0.3 (e).

ported to be active [22]. In contrast, Pt–Co/SiO_2 (Pt/Co = 3) gave higher conversions at 413 and 453 K than any other catalysts, with significant conversions even at lower temperatures. A separate run on Co (5 wt%)/SiO_2 gave much lower activity, with 16% CO conversion, at 453 K. Based on these findings, we conclude that Pt–Co/SiO_2 (Pt/Co = 3) is the most effective Pt–Co/SiO_2 catalyst for the PROX reaction.

To identify the active IMCs, XRD patterns were obtained for the Pt–Co/SiO_2 catalysts, as shown in Fig. 4. The addition of Co onto Pt/SiO_2 (a) gradually shifted the peak position to greater angles in (b) and (c), suggesting the formation of a solid solution between Pt and Pt_3Co. At a Pt/Co ratio of 3 (d), the peak appeared at almost the same position as that of Pt_3Co (40.5°), as indicated by the dotted line. Further addition of Co (Pt/Co = 1) generated the diffraction from PtCo (e). The Co-rich catalyst (Pt/Co = 1/4) showed no significant XRD pattern, indicating the absence of an IMC phase. Based on the results shown in Figs. 3 and 4, we conclude that Pt_3Co was the most effective IMC for the PROX reaction in a wide temperature range, whereas PtCo had greater activity but lower selectivity. The high activity of Pt–Co bimetallic catalysts has already been reported on TiO_2 [19], Al_2O_3 [20], and YSZ [22]; however, the contribution of Pt_3Co IMC was first revealed in the present study.

We also studied the combination of Pt–Cu in a manner similar to that for Pt–Co described earlier. Fig. 5 shows the results of the reaction on Pt–Cu/SiO_2 with Pt/Cu ratios of 0.3, 1, 2, and 5. Pt–Cu/SiO_2 with Pt/Cu = 1 gave the highest conversion at almost all temperatures studied, whereas Pt–Cu/SiO_2 with Pt/Cu = 5 gave a much lower conversion, comparable to that on Pt/SiO_2. Cu (5 wt%)/SiO_2 also gave low activity, with 18% CO conversion at 450 K. Fig. 6 shows XRD patterns for Pt–Cu/SiO_2. The addition of Cu on Pt/SiO_2 (a) shifted the diffraction peak to a greater angle. Because Pt and Cu will form a solid solution with any com-

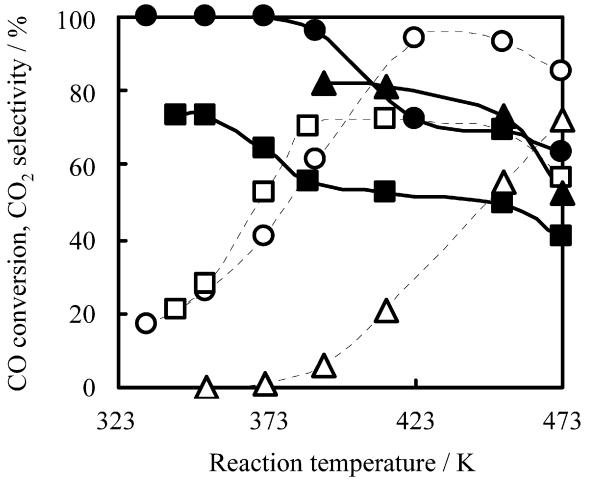

Fig. 7. CO_2 selectivity (solid symbols) and CO conversion (open symbols) of Pt_3Co/SiO_2 (●,○), $PtCu/SiO_2$ (■,□) and Pt/SiO_2 (▲,△). Reactant mixture: CO (2.0%), O_2 (1.3%), H_2 (35%) and He (balance).

position at higher temperatures, the solid solution between Pt–Cu alloy and PtCu IMC may be formed in these catalysts. Pt–Cu/SiO_2 with Pt/Cu = 1 (d) gave the diffraction in almost the same position as that of PtCu (41.0°). Pt–Cu/SiO_2 with Pt/Cu = 0.3 (e) gave the diffraction from $PtCu_3$. Based on these findings, we conclude that PtCu was the most effective IMC between Pt and Cu for the PROX reaction at a wide temperature range.

Fig. 7 shows the CO_2 selectivity of the active catalysts, Pt_3Co/SiO_2 and $PtCu/SiO_2$, together with that of Pt/SiO_2 at various temperatures. Pt_3Co/SiO_2 showed almost 100% selectivity to CO_2 at low temperatures, indicating that oxygen was used only for the oxidation of CO; that is, no hydrogen consumption occurred on Pt_3Co. Although CO_2 selectivity decreased at higher temperatures, it remained around 70% at 453 K, where CO conversion was >95%. $PtCu/SiO_2$ gave lower selectivity than Pt_3Co/SiO_2 even at low temperatures. Its selectivity was comparable to that of Pt/SiO_2 at a similar conversion level. Clearly, due to its high selectivity and high activity, Pt_3Co/SiO_2 is a better catalyst than $PtCu/SiO_2$ for the PROX reaction.

The surface of IMCs, such as $LaNi_5$ and $ThNi_5$, changes during the hydrogenation of CO from IMC phase to Ni metallic particles and a thin layer of La_2O_3 or ThO_2 [28]. When the reactant contains oxygen atoms, such segregation into pure metal and oxide phases can occur if one component element has a greater affinity to oxygen than the other. Moreover, the complete oxidation into oxide phases can occur if both elements have a high affinity. Consequently, we studied the stability of Pt_3Co/SiO_2 and $PtCu/SiO_2$ under the stated reaction conditions. Fig. 8 shows XRD patterns of Pt_3Co/SiO_2 and $PtCu/SiO_2$ before and after the PROX reaction at a constant temperature of 413 K for 4 h. At this temperature, CO conversion on both catalysts exceeded 80%. The diffraction peaks of Pt_3Co (1-A, B) and PtCu (2-A, B) did not change significantly, and no diffractions from other oxide species were observed, indicating no segregation in bulk of IMC phases during the reaction. To clarify the surface segregation during the PROX reaction at high temperatures, the reaction was repeated on the same catalyst, as shown in Fig. 9. The reaction was carried out from 333 to 473 K in the first run, after which the temperature was decreased to 333 K in the flow of reactant and the reaction was repeated to 473 K in the second run. For both catalysts, CO conversion in the second run closely replicated that in the first run. The Pt_3Co and PtCu surfaces did not change irreversibly during the reaction at higher temperatures, suggesting that no surface segregation of these IMCs

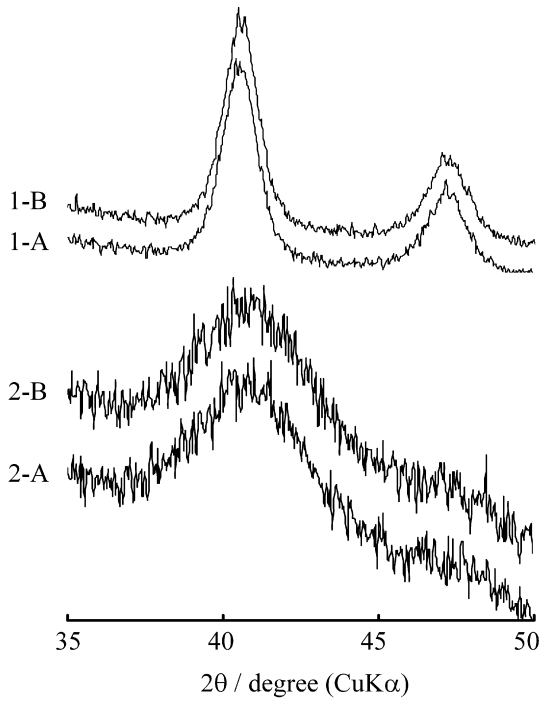

Fig. 8. XRD patterns of Pt_3Co/SiO_2 (1) and $PtCu/SiO_2$ (2) before (B) and after (A) the PROX of CO at 413 K for 4 h.

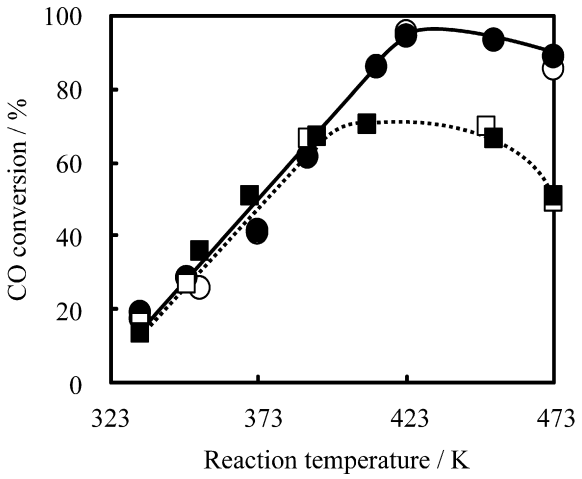

Fig. 9. CO conversion in the first run (open symbols) and the subsequent second run (solid symbols) on Pt_3Co/SiO_2 (●,○) and $PtCu/SiO_2$ (■,□). Reactant mixture: CO (2.0%), O_2 (1.3%), H_2 (35%) and He (balance).

occurred and that Pt_3Co and PtCu were stable under the reaction conditions.

3.3. Characterization of Pt_3Co/SiO_2 and $PtCu/SiO_2$

In this section, we explore why Pt_3Co/SiO_2 and $PtCu/SiO_2$ exhibited greater activity than Pt/SiO_2 for the PROX reaction, presenting some characterization results. First, we performed TEM on these catalysts to determine the particle sizes of the metals and IMCs. Fig. 10 shows TEM images of three catalysts obtained with the same magnification. Pt/SiO_2 (a) was composed of a few large particles with numerous highly dispersed small particles. The particle size distribution, shown in Fig. 11 in solid bars, was mainly 1–3 nm. Fig. 10b shows that $PtCu/SiO_2$ comprised larger particles than Pt/SiO_2, with most particles in the range of 2–5 nm. Pt_3Co/SiO_2 had larger particles than $PtCu/SiO_2$. Based on the XRD

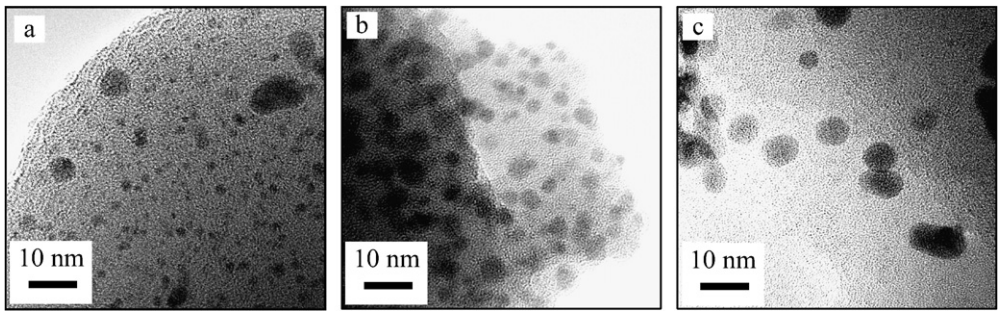

Fig. 10. TEM images of Pt/SiO_2 (a), $PtCu/SiO_2$ (b) and Pt_3Co/SiO_2 (c).

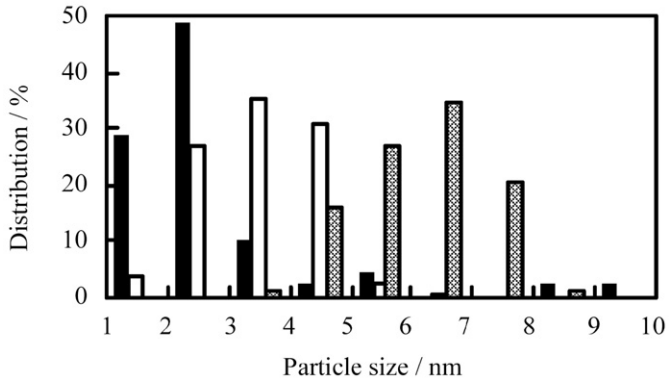

Fig. 11. Distribution of metal particle size in Pt/SiO_2 (solid bars), $PtCu/SiO_2$ (open bars) and Pt_3Co/SiO_2 (shaded bars).

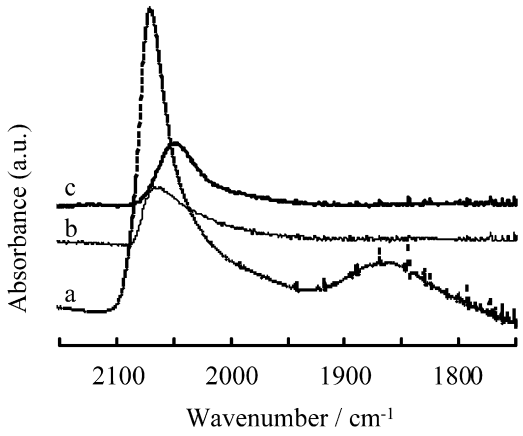

Fig. 12. IR spectra of CO adsorbed on Pt/SiO_2 (a), Pt_3Co/SiO_2 (b) and $PtCu/SiO_2$ (c).

patterns, the crystallite sizes of these catalysts were estimated as <4 nm for Pt/SiO_2 and $PtCu/SiO_2$ and 6 nm for Pt_3Co/SiO_2. The rough agreement between particle size determined by TEM and crystallite size determined by XRD would exclude the presence of amorphous metal particles and polycrystalline particles on silica. Based on these results, we conclude that the higher activity of Pt_3Co/SiO_2 and $PtCu/SiO_2$ compared with that of Pt/SiO_2 is not associated with the greater dispersion of these IMCs; rather, the intrinsic activity of Pt_3Co and PtCu must be higher than that of Pt.

We also investigated the catalyst surfaces by evaluating the IR spectra of adsorbed CO. As shown in Fig. 12, CO adsorbed on Pt/SiO_2 at 298 K gave a main absorption band attributed to linear CO at around 2050 cm^{-1} and a weak band attributed to bridged CO at around 1850 cm^{-1}. Pt_3Co/SiO_2 and $PtCu/SiO_2$ gave only a band at around 2050 cm^{-1} attributed to linear CO adsorbed on Pt atoms in IMCs. The disappearance of bridged CO indicates that the distance between adjacent Pt atoms on the surface of IMCs is longer than that on pure Pt. This could be evidence of the formation of IMC phases on the surface of Pt_3Co and PtCu particles as well as in their bulk, as was confirmed by XRD (see Figs. 4 and 6). The disappearance of bridged CO was also found for Ni_3Sn, Ni_3Sn_2, and Ni_3Sn_4 on SiO_2 [29]. Moreover, the intensity of the linear CO band on the IMC catalysts was significantly lower than that on the Pt catalysts. The adsorption of CO is weakened by IMC formation. The strong adsorption of CO on Pt hinders the adsorption of O_2, resulting in low PROX activity at low temperatures. The weaker adsorption of CO on IMCs may be the reason why Pt_3Co/SiO_2 and $PtCu/SiO_2$ exhibited greater PROX activity than Pt/SiO_2. The amount of CO adsorbed at 298 K was 86 $\mu mol\,g^{-1}$ on Pt/SiO_2, 11 $\mu mol\,g^{-1}$ on Pt_3Co/SiO_2, and 10 $\mu mol\,g^{-1}$ on $PtCu/SiO_2$. As expected based on the TEM results (Fig. 10), the uptakes on the IMC catalysts were much lower than those on Pt/SiO_2. We calculated the TOFs for the formation of CO_2 based on the CO uptake. The TOFs on Pt_3Co/SiO_2 and $PtCu/SiO_2$ were 0.84 and 0.52 s^{-1}, respectively, at the reaction temperature of 353 K. These values are much higher than the 0.032 s^{-1} reported for $K–Pt/Al_2O_3$ in the PROX reaction at 363 K [30].

The IR peak position of linear CO shifted to a lower wavenumber when some of the adsorbed CO molecules were desorbed by evacuation. The final peak position after successive evacuation was almost the same (ca. 2048 cm^{-1}) for the three catalysts. Because the electronic state of the surface Pt atoms could not be clarified accurately because of the repulsive interaction between adsorbed CO molecules, we studied the electronic (ligand) effect through the formation of IMCs by XPS. Fig. 13 shows XPS spectra of Pt 4f (a), Co 2p (b), and Cu 2p (c) in pure metal foils and also of unsupported Pt_3Co (d) and PtCu (e). Because the intensity of Co 2p peaks in Pt_3Co/SiO_2 was too weak to allow us to estimate the oxidation state and surface composition, here we used unsupported IMC powders prepared by the arc-melting technique [9]. Table 1 gives the binding energies obtained from the XPS spectra. The Pt $4f_{7/2}$ peaks in Pt_3Co and PtCu gave slightly higher binding energies than that seen for Pt foil. Pt atoms on the surface of Pt_3Co and PtCu were found to be positively charged compared with those on pure Pt metal. Pt $4f_{7/2}$ peaks in Pt_3Co/SiO_2, $PtCu/SiO_2$, and Pt/SiO_2 appeared at 74.1, 74.2, and 73.9 eV, respectively. The similar positive shifts in Pt $4f_{7/2}$ binding energy for unsupported IMCs also were found for SiO_2-supported IMCs; however, these binding energies were greater than those for bulk IMCs due to the small particle size of the supported catalysts. The electron-deficient Pt atoms on IMCs weakly adsorbed CO compared with those on pure Pt due to the decreased back-donation from Pt to CO. This corresponds to the results for CO adsorption obtained by IR and CO uptake measurements. The ligand effect of IMC formation was found to affect the catalytic activity for the PROX reaction, as well as the ensemble effect revealed by the IR spectra. As shown in Table 1, the Cu $2p_{3/2}$ peak appeared at a lower binding energy in PtCu than in Cu foil, indicating the electron transfer from Pt to Cu in PtCu, although the appreciable change in Co $2p_{3/2}$ peak position was not observed in

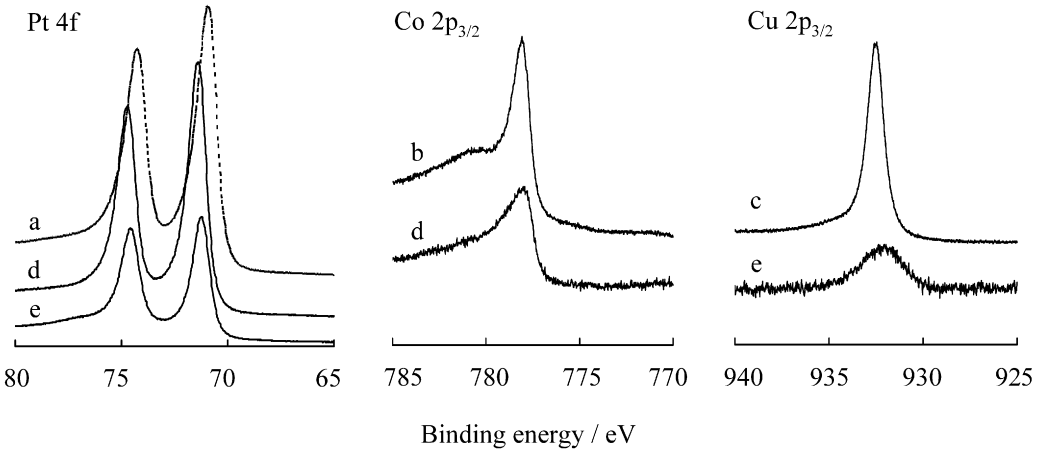

Fig. 13. XPS spectra of Pt 4f, Co $2p_{3/2}$ and Cu $2p_{3/2}$ in foils of Pt (a), Co (b) and Cu (c) and unsupported Pt_3Co (d) and PtCu (e).

Table 1
Results of XPS measurement on unsupported catalysts

Catalyst	Binding energy (eV)			Surface composition	
	Pt $4f_{7/2}$	Co $2p_{3/2}$	Cu $2p_{3/2}$	Pt/Co	Pt/Cu
Pt foil	70.9	–	–	–	–
Co foil	–	778.1	–	–	–
Cu foil	–	–	932.5	–	–
Pt_3Co	71.3	778.1	–	4	–
PtCu	71.2	–	932.1	–	1.1

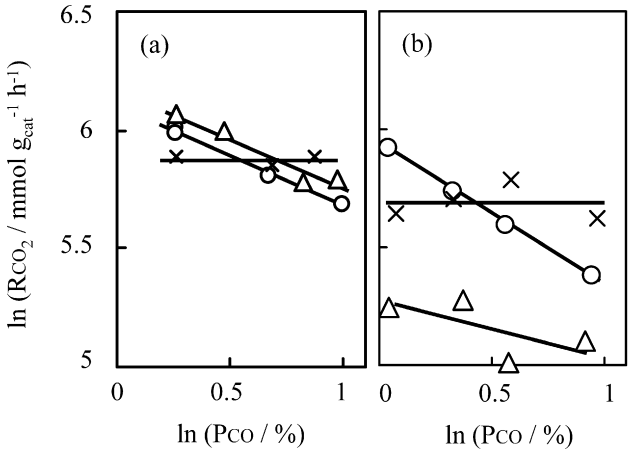

Fig. 14. Effect of CO partial pressure on the rate of CO_2 formation at 413 K on Pt/SiO_2 (×) and at 333 K on Pt_3Co/SiO_2 (○) and $PtCu/SiO_2$ (△) with H_2 (a) and without H_2 (b).

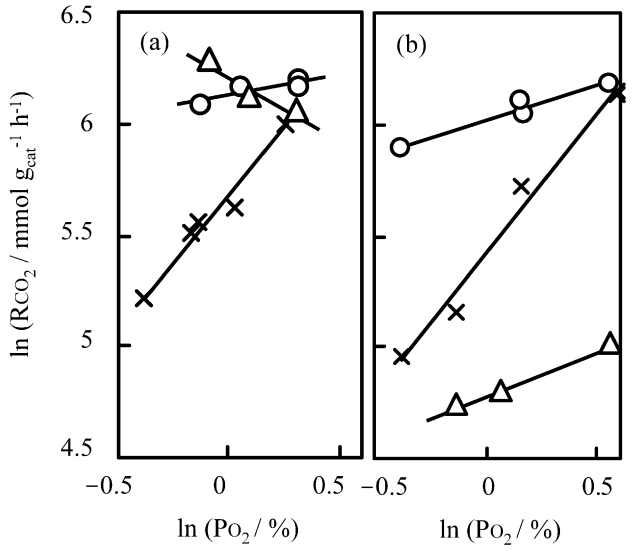

Fig. 15. Effect of O_2 partial pressure on the rate of CO_2 formation at 413 K on Pt/SiO_2 (×) and at 333 K on Pt_3Co/SiO_2 (○) and $PtCu/SiO_2$ (△) with H_2 (a) and without H_2 (b).

the formation of Pt_3Co. Lee et al. [31] reported a positive shift in Pt $4f_{7/2}$ and negative shifts in Co $2p_{3/2}$ and Cu $2p_{3/2}$ for bulk Pt_3Co and PtCu, but no significant shift of Pt $4f_{7/2}$ in PtCu. In the case of Pt_3Ge, however, we detected the electron transfer from Ge to Pt by XPS [9]. The composition near the surface of IMCs was estimated from the XPS spectra, as shown in Table 1. On both IMCs, the surface compositions were comparable to the bulk ones, Pt/Co = 3 and Pt/Cu = 1. The enrichment in one element on the surface did not occur on both IMCs. This also provides evidence of the formation of IMC phase on the surface of Pt_3Co and PtCu, in addition to the disappearance in bridged CO.

We carried out kinetic studies to help clarify the adsorption of reactant molecules under the stated reaction conditions. Figs. 14 and 15 show the effect of partial pressures of CO and O_2, respectively, on the rate of CO_2 formation in the presence (a) or absence (b) of hydrogen. The reaction temperatures were adjusted to 413 K for Pt/SiO_2 and to 333 K for the IMC catalysts to obtain CO conversions of 5–10%. In the case of Pt/SiO_2, the reaction order was estimated to be 0 with respect to P(CO) and 1 with respect to $P(O_2)$, irrespective of the presence or absence of hydrogen. The CO adsorption must be saturated on the surface of Pt; therefore, the reaction may proceed mainly through the Rideal mechanism with the reaction between the adsorbed CO and gaseous O_2. In contrast, the reaction order with respect to P(CO) was not 0 for both IMC catalysts, indicating that CO adsorption is not saturated. The reaction proceeded through the Langmuir–Hinshelwood mechanism, as has been proposed on Pt–Fe/mordenite [32]. In the case of Pt_3Co/SiO_2, the reaction order with respect to $P(O_2)$ was positive both with and without hydrogen. CO adsorption was stronger than O_2 adsorption irrespective of the presence or absence of hydrogen. Oxygen was adsorbed mainly on Co, because the IR spectra did not indicate CO adsorption on Co. The CO molecules on Pt would be oxidized by oxygen atoms activated on Co, resulting in higher activity of Pt_3Co compared with Pt metal. Other researchers have reported on the adsorption site for oxygen in the PROX reaction, for example, Sn or SnO_x in $Pt–Sn/Al_2O_3$ [17], Nb_2O_5 support in $Pt–Sn/Nb_2O_5$ [18], and Fe in Pt–Fe/mordenite [32]. In the case of $PtCu/SiO_2$, however, the reaction order with respect to $P(O_2)$ was negative in the presence of hydrogen (Fig. 15a) but posi-

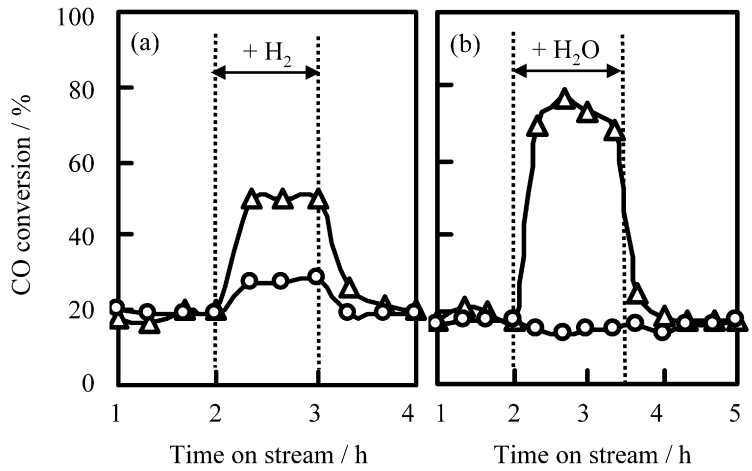

Fig. 16. Effect of H_2 (35%, a) and H_2O (10%, b) on the oxidation of CO at 353 K on Pt_3Co/SiO_2 (○) and $PtCu/SiO_2$ (△) with the reactant mixture of CO (2.0%), O_2 (1.0%) and He (balance).

tive without hydrogen. As a result, the adsorptions of CO and O_2 were almost comparable in the presence of hydrogen. Hydrogen enhanced the adsorption of O_2. Comparing CO_2 formation rates obtained with and without hydrogen reveals that the activity of Pt and Pt_3Co increased slightly and that of PtCu increased significantly with the addition of hydrogen. Hydrogen contributed to the high PROX activity of $PtCu/SiO_2$ at low temperatures.

We also studied the enhancing effect of hydrogen on the PROX reaction in the steady-state reaction. Fig. 16 shows the effect of adding hydrogen and water to the reactant containing CO and O_2. It should be noted that the O_2 concentration was lower than that in the cases shown in Figs. 2, 3, and 5. On Pt_3Co/SiO_2, CO conversion was increased slightly by the addition of hydrogen but was not increased by the addition of water. The weak enhancing effect was caused by the hydrogen itself. On $PtCu/SiO_2$, however, CO conversion increased by 30% with the addition of hydrogen and even further by the addition of water. The enhancing effect of hydrogen reflected the contribution of water produced by the oxidation of hydrogen during the PROX reaction. As shown in Fig. 7, the oxidation of hydrogen occurred on $PtCu/SiO_2$ at all temperatures studied, supplying the water molecules necessary to enhance CO_2 formation. The formation of CO_2 in the presence of water could be caused by the CO shift reaction. We carried out the reaction of CO (2%), H_2O (10%), and H_2 (35%) in a helium carrier on $PtCu/SiO_2$ and found no CO_2 formation in the temperature range of 333–473 K. The CO shift reaction is negligible during the PROX reaction. The increase in CO_2 formation rate by the addition of water results from the acceleration of O_2 adsorption to oxidize CO. Such an enhancing effect of water has been reported for $Pt–Pd/CeO_2$ [4] and $FeO_x/Pt/TiO_2$ [33]. The water molecules adsorbed on Cu may react with adjacent CO on Pt to form a carboxyl group [33], which may accelerate the adsorption of oxygen to oxidize CO into CO_2. The participation of water molecules in the PROX reaction on PtCu is the reason for its lower selectivity compared with Pt_3Co. The change in CO conversion was fast for both the addition and removal of hydrogen; therefore, PtCu was stable in the absence of hydrogen, without the phase segregation caused by the oxidation of copper.

4. Conclusion

This study has investigated the catalytic properties of Pt-based IMC catalysts for the PROX reaction. The active species for PROX at low temperatures were Pt_3Co, PtCo, and PtCu. These IMCs supported on silica exhibited greater activity than Pt/SiO_2 and were stable under the stated reaction conditions up to 473 K. Their high activity is related to the ready adsorption of oxygen under the reaction conditions compared with the surface of pure Pt. The formation of IMCs induced an extension of the Pt–Pt atomic distance (geographic effect) and an electron transfer from Pt to Co or Cu (electronic effect). Both of these effects resulted in the weaker adsorption of CO on the IMC surface compared with on the Pt surface. Pt_3Co was found to have high selectivity for CO_2 formation. PtCu had a slightly lower selectivity, because on PtCu the formation of small amounts of water through the oxidation of hydrogen is necessary for the oxidation of CO at low temperatures.

Acknowledgments

This work was supported in part by Grant-in-Aid 17560680 from the Japanese Ministry of Education, Science, Sports and Culture. The authors thank Professor Takeyama for IMC preparation, Professor Yano for the XPS measurements, and Dr. Takagi and Mr. Genseki (Center for Advanced Materials Analysis, Tokyo Institute of Technology) for the TEM measurements.

References

[1] S.H. Oh, R.M. Sinkevitch, J. Catal. 142 (1993) 254.
[2] S.Y. Chin, O.S. Alexeev, M.D. Amiridis, J. Catal. 243 (2006) 329.
[3] P. Naknam, A. Luengnaruemitchai, S. Wongkasemjit, S. Osuwan, J. Power Sources 165 (2007) 353.
[4] A. Parinyaswan, S. Pongstabodee, A. Luengnaruemitchai, Int. J. Hydrogen Energy 31 (2006) 1942.
[5] E.Y. Ko, E.D. Park, K.W. Seo, H.C. Lee, S. Kim, Catal. Lett. 110 (2006) 275.
[6] Binary Alloy Phase Diagrams, second ed., ASM International and National Institute of Standards and Technology, 1990, pp. 415, 2844, 3034 and 3123.
[7] W.E. Wallace, Chemtech 12 (1982) 752.
[8] T. Komatsu, M. Fukui, T. Yashima, Stud. Surf. Sci. Catal. 101 (1996) 1095.
[9] T. Komatsu, S. Hyodo, T. Yashima, J. Phys. Chem. B 101 (1997) 5565.
[10] A. Onda, T. Komatsu, T. Yashima, Phys. Chem. Chem. Phys. 2 (2000) 2999.
[11] T. Komatsu, M. Mesuda, T. Yashima, Appl. Catal. A 194–195 (2000) 333.
[12] A. Onda, T. Komatsu, T. Yashima, J. Catal. 201 (2001) 13.
[13] T. Komatsu, D. Satoh, A. Onda, Chem. Commun. (2001) 1080.
[14] T. Komatsu, K. Inaba, T. Uezono, A. Onda, T. Yashima, Appl. Catal. A 251 (2003) 315.
[15] T. Komatsu, Y. Fukui, Appl. Catal. A 279 (2005) 1730.
[16] T. Komatsu, H. Ikenaga, J. Catal. 241 (2006) 426.
[17] M.M. Schubert, M.J. Kahlich, G. Feldmeyer, M. Hüttner, H.A. Hackenberg, H.A. Gasteiger, R.J. Behm, Phys. Chem. Chem. Phys. 3 (2001) 1123.
[18] P. Marques, N.F.P. Ribeiro, M. Schmal, D.A.G. Aranda, M.M.V.M. Souza, J. Power Sources 158 (2006) 504.
[19] W.S. Epling, P.K. Cheekatamarla, A.M. Lane, Chem. Eng. J. 93 (2003) 61.
[20] P.V. Snytnikov, K.V. Yusenko, S.V. Korenev, Yu.V. Shubin, V.A. Sobyanin, Kinet. Catal. 48 (2007) 276.
[21] C. Kwak, T.J. Park, D.J. Suh, Appl. Catal. A 278 (2005) 181.
[22] E.Y. Ko, E.D. Park, H.C. Lee, D. Lee, S. Kim, Angew. Chem. Int. Ed. 46 (2007) 734.

[23] M. Watanabe, H. Uchida, K. Ohkubo, H. Igarashi, Appl. Catal. B 46 (2003) 595.
[24] M. Kotobuki, A. Watanabe, H. Uchida, H. Yamashita, M. Watanabe, Appl. Catal. A 307 (2006) 275.
[25] M. Shou, K. Tanaka, K. Yoshioka, Y. Moro-oka, S. Nagano, Catal. Today 90 (2004) 255.
[26] Binary Alloy Phase Diagrams, second ed., ASM International and National Institute of Standards and Technology, 1990, p. 1226.
[27] Binary Alloy Phase Diagrams, second ed., ASM International and National Institute of Standards and Technology, 1990, p. 1461.
[28] H. Imamura, W.E. Wallace, J. Phys. Chem. 84 (1980) 3145.
[29] A. Onda, T. Komatsu, T. Yashima, J. Catal. 221 (2003) 378.
[30] M. Kuriyama, H. Tanaka, S. Ito, T. Kubota, T. Miyao, S. Naito, K. Tomishige, K. Kunimori, J. Catal. 252 (2007) 39.
[31] Y.S. Lee, K.Y. Lim, Y.D. Chung, C.N. Whang, Y. Jeon, Surf. Interface Anal. 30 (2000) 475.
[32] M. Kotobuki, A. Watanabe, H. Uchida, H. Yamashita, M. Watanabe, J. Catal. 236 (2005) 262.
[33] K. Tanaka, M. Shou, H. He, X. Shi, Catal. Lett. 110 (2006) 185.